Article type: Article

Terthieno[3,2-*b*]thiophene (6T) based low band-gap fused-ring electron acceptor for high efficiency solar cell with a high short-circuit current density and low open-circuit voltage loss

Xueliang Shi[a,†], Jingde Chen[a,e†], Ke Gao[a,†], Lijian Zuo[a], Zhaoyang Yao[a], Feng Liu[c], Jianxin Tang*[e], Alex K-Y. Jen*[a,b]*

Dr. X. Shi, J. Chen, Dr. K. Gao, Dr. L. Zuo, Dr. Z. Yao, Prof. A. K.-Y. Jen
[a]Department of Materials Science and Engineering, University of Washington, Seattle, WA, 98195-2120, USA

Prof. A. K.-Y. Jen
[b]Department of Chemistry, City University of Hong Kong, Kowloon, Hong Kong

Prof. F. Liu
[c]Department of Physics and Astronomy, Shanghai Jiaotong University, Shanghai 200240, China

J. Chen, Prof. J. Tang

[d]Institute of Functional Nano & Soft Materials (FUNSOM), Collaborative Innovation Center of Suzhou Nano Science and Technology, Jiangsu Key Laboratory for Carbon-Based Functional Materials & Devices, Soochow University, Suzhou 215123, China

*Corresponding authors. E-mail: ajen@uw.edu, fengliu82@sjtu.edu.cn, jxtang@suda.edu.cn

[†]These authors contribute to this work equally.

WILEY-VCH

Abstract: A terthieno[3,2-*b*]thiophene (**6T**) based fused-ring low bandgap electron acceptor, **6TIC**, has been designed and synthesized for highly efficient non-fullerene solar cells. The chemical, optical & physical properties, device characteristics, and film morphology of **6TIC** have been intensively studied. **6TIC** showed a narrow bandgap with band edge reaching 905 nm due to the electron-rich π-conjugated **6T** core and reduced resonance stabilization energy. The rigid, π-conjugated **6T** also offers lower reorganization energy to facilitate very low V_{OC} loss in 6TIC system. The analysis of film morphology showed that **PTB7-Th** and **6TIC** can form crystalline domains and bicontinous network. These domains were enlarged when thermal annealing was applied. Consequently, the device based on **PTB7-Th:6TIC** exhibits a high power conversion efficiency (PCE) of 11.07% with a high $J_{SC} > 20$ mA/cm^2 and a high V_{OC} of 0.83 V with relatively a low V_{OC} loss (~ 0.55 V). Moreover, a semitransparent solar cell based on **PTB7-Th:6TIC** exhibits a relatively high PCE (7.62%). The device can have combined high PCE and high J_{SC} is quite rare for organic solar cells.

1. Introduction

Recently, non-fullerene acceptors (NFAs) have attracted great attention and undergone a rapid development as active materials for high-performance organic solar cells (OSCs) in renewable energy applications.[1-2] Among the reported NFAs, one of the most successful examples is the development of fused-ring electron acceptors (FREAs) such as the benchmark molecules **IEIC** and **ITIC**.[3-4] The prevalent FREAs based on planar acceptor-donor-acceptor (A-D-A) system with strong intramolecular charge transfer (ICT) facilitates π-electron delocalization and reduces bandgap. Consequently, it endows the acceptors with extended light absorption to efficiently harvest photons to increase short circuit current (J_{SC}) (**Figure 1**).[5] The rigid and planar FREAs with strong inter-molecular interaction (π-π stacking) can also reduce rotational molecular disorder and reorganization energy to result in

WILEY-VCH

enhanced charge carrier mobilities and low open circuit voltage (V_{OC}) loss ($V_{OC\ loss} = eE_g^{OPT} - V_{OC}$).[6] Most recently, significant efforts have been devoted to developing more efficient FREAs by manipulating HOMO/LUMO energy levels, broadening absorption bands, and controlling intermolecular interactions and morphology. For example, through exquisitely utilizing different central donors, acceptors, and spacers, various highly efficient FREAs have been developed to reach PCE over 10%.[7-23] Actually, the certificated PCE of state-of-the-art FREA-based OSCs has already reached 13%, which is a benchmark value for all OSCs.[24-25]

Among numerous encouraging results reported so far for FREAs, a very challenging task is to develop low bandgap (<1.5 eV) FREAs that can simultaneously possess near-infrared (NIR) absorption (>800 nm) and high device performance. Low bandgap FREAs have several great merits due to their distinc properties. First, their absorbance can better match with solar spectrum to generate photocurrent, which is an effective way to enhance J_{SC} and PCE. Second, they can be incorporated into semitransparent OSCs to exhibit high transparency in visible light and high light-to-electricity conversion. Third, they can be used in back sub-cell of a tandem solar cell.

The common approaches for developing low band-gap FREAs are based on either decreasing their LOMO energy levels or elevating their HOMO energy levels which however is detrimental to V_{OC}. For example, the extension of FREA photo-response range to NIR by decreasing its LUMO energy level often causes significant V_{OC} loss. On the token, up shifting HOMO energy level of FREA will diminish the HOMO energy offset between the acceptor and donor to reduce hole transfer and photocurrent generation. To date, most of the NIR OSC devices with J_{SC} higher than 20 mA/cm^2 usually display very low V_{OC} (< 0.5V) with a high V_{OC} loss (> 0.6V), resulting a modest PCE ~ 5-6%.[26] Therefore, it is quite challenging to design novel low bandgap FREAs that can simultaneously maintain high J_{SC} and V_{OC} to result in desirable PCE (> 10%).

One of the most effective and straightforward strategies for low bandgap FREAs is to increase the donating ability of central donor to enhance the ICT effect. For example, Hou *et al.* have

successfully demonstrated an efficient low band-gap FREA by introducing alkoxy groups onto **IEIC** to result in much narrower bandgap with NIR absorption.[27-28] By introducing quinoidal structure to extend the effective π-conjugation length, Zhu *et al.* have also developed an efficient low bandgap FREA to realize efficient semitransparent OSC.[29] Recently, our group have developed a thiophene-thieno[3,2-*b*]thiophene-thiophene (**4T**) based low bandgap FREA **4TIC**, showing in addition to electron-donating ability and conjugation length, the resonance stabilization energy of central donor can also significantly contribute to the ICT effect to shift the absorption edge of FREAs towards NIR.[30] Base on this work, the **4T** unit is further extended to terthieno[3,2-*b*]thiophene (**6T**) by incorporating two more thieno[3,2-*b*]thiophene (TT) units, which can be end-capped with 3-(dicyanomethylidene)-indan-1-one (**IC**) acceptor to form a novel low bandgap FREA, **6TIC** (**Figure 1**).

The evolution from **4T** to **6T** endows the designed **6TIC** with several distinct advantages in optical and electrical properties as well as its application in OSCs. For instance, the rigid fused terthieno[3,2-*b*]thiophene **6T**, like **4T** core, will allow more efficient π-electron delocalization than the commonly used indacenothiophene (IDT) or indacenodithieno[3,2-*b*]thiophene (IDTT) core due to its lower resonance stabilization energy.[30] Furthermore, **6T** has longer effective conjugation length than **4T**, which can induce stronger ICT when combine with terminal **IC** acceptor to further extend the absorption of **6TIC** to NIR. The **6TIC** with two outward TT units can also enhance the planarity of the **6TIC** framework, leading to more efficient molecular packing and charge transport. As expected, the **6TIC** thin film shows an intense and broadened absorption between 600 and 900 nm with an onset at ~905 nm. Compared with **4TIC**, **6TIC** has a higher lying HOMO energy level and a slightly smaller bandgap. **6TIC** also shows superior electron mobility than that of **4TIC**. As a result, the devices based on **6TIC** exhibit a high PCE (11.07%) with a high J_{SC} (>20.00 mA/cm^2), and a high

V_{OC} of 0.83 V with a relatively low V_{OC} loss (0.55 V). The semitransparent solar cell based on **6TIC** also

exhibits a quite high PCE (7.67%). The combined high PCE and J_{SC} is quite rare in OSCs reported so far

which validates the effectiveness of molecular design.

2. Results and Discussion

The synthetic procedures of **6T** and **6TIC** are similar to those of our reported **4TIC** which is depicted in **Figure 1b**. The Stille coupling between diethyl 2,5-dichlorothieno[3,2-*b*]thiophene-3,6-dicarboxylate **1**[31-32] and tributyl(thieno[3,2-*b*]thiophen-2-yl)stannane **2** gave diester **3** in over 90% yield. The double nucleophilic additions of (4-hexylphenyl)magnesium bromide Grignard regent to diester **3**, followed by amberlyst 15 induced Friedel−Crafts intramolecular cyclization afford **6T** in 75% yield. It was noted that the commonly used conditions for Friedel-Crafts intramolecular cyclization such as protic acid (acetic acid/HCl and acetic acid/H_2SO_2) or Lewis acid (BF_3 etherate) catalyzed ring closure can only give **6T** in very low yields. **6T** was then treated with Vilsmeier reagent to afford the di-carbaldehyde **6T-CHO** in 93% yield. Finally, **6TIC** was obtained as a deep blue color solid in 91% yield by Knoevenagel condensation reactions between **6T-CHO** and **IC**. All the new compounds were fully characterized by ^{1}H NMR, ^{13}C NMR and mass spectrometry (see Supporting Information (SI)).

The UV-vis-NIR absorption spectra of **6TIC** were recorded in dichloromethane (DCM) solution and in solid state, and were compared with those of reported **4TIC** (**Figure 2a**). In solution, **6TIC** exhibits a strong absorption peak in the region between 600 and 850 nm with an onset at 846 nm, which red-shifted considerably compared to that of **4TIC** (band edge at 806 nm). In the solid state, **6TIC** thin film further red-shifted to NIR with the absorption edge at 905 nm, whereas **4TIC** has an absorption edge at 886 nm. **6TIC** also shows much broader absorption than **4TIC** in both solution and solid state. Moreover, the absorption band profile of **6TIC** differs from that of **4TIC** in solid state, with **6TIC** displays two comparative absorption peaks compared to **4TIC,** which only shows a main absorption peak and a high-energy shoulder. The NIR absorption of **6TIC** is expected to improve light utilization and contribute to higher J_{SC} in OSC.

The electrochemical properties of **6TIC** were investigated by cyclic voltammetry (CV) in dry DCM solution and compared with **4TIC** (**Figure 2b**). **6TIC** exhibits one irreversible reductive wave and two reversible oxidative waves with the half-wave potential $E_{1/2}^{OX}$ at 0.43 V, 0.85 V (*vs.* Fc$^+$/Fc, Fc: ferrocene). Compared to **6TIC**, **4TIC** also exhibits one irreversible reductive wave but only one reversible oxidative waves with the half-wave potential $E_{1/2}^{OX}$ at 0.56 V. The HOMO and LUMO energy levels determined from the onset of the first oxidative and reductive waves, respectively, are summarized in **Table 1**. Compared with **4TIC**, **6TIC** has a higher lying HOMO energy level of -5.21 eV, which is attributed to the more electron- rich nature of **6T**. It also induces stronger ICT with terminal **IC** group resulting in slightly lifted LOMO energy level of **6TIC** compared to **4TIC**. The bandgap of **6TIC** was thus determined to be 1.38 eV, which is in accordance with its optical bandgap of 1.37 eV, calculated from its absorption edge (905 nm). Therefore, **6TIC** has a slightly smaller band-gap than **4TIC** based on both optical and electrochemical measurements, which is ascribed to the longer π-conjugation length and more electron-rich nature of **6T**.

5

WILEY-VCH

Density functional theory (DFT) calculations at the B3LYP/6-31G(d,p) level were employed to further understand the difference between **4TIC** and **6TIC**. The change of central donor from **4T** to **6T** does not have significant impact on the electron density distributions. For both molecules, the electron densities of HOMO are mainly localized at the central **4T** or **6T** unit, whereas those of LUMO are homogeneously distributed along the quinoidal conjugation to the terminal acceptor unit, suggesting very efficient ICT in these   A-D-A systems (**Figure 2c**). However, different central donors in **4TIC** and **6TIC** result in different HOMO and LUMO energy levels. Particularly, the calculated HOMO of **6TIC** is much higher than that of **4TIC** while its LUMO level is slightly higher than **4TIC**, leading to a narrower band-gap of **6TIC**. The trend of the calculated HOMO and LUMO change is consistent with the findings from the electrochemical studies of **6TIC**.

To investigate the photovoltaic properties of **6TIC**, the commercially available **PTB7-Th** is used as the donor polymer to fabricate OSCs using the device configuration of ITO/ZnO/**PTB7-Th**:**6TIC**/MoO$_3$/Ag, where ITO is indium tin oxide. It was found that the donor/acceptor weight ratio of 1:1.5 in chlorobenzene solution with 0.25% diiodooctane (DIO) as additive gave the best device performance after optimizing with different processing solvents, donor/acceptor ratio, thickness, and DIO addictive ratio. As shown in **Figure 3a** and **Table 2**, devices based on the as-cast **PTB7-Th:6TIC** film under the above optimized condition gave a promising PCE of 9.72% with a Voc of 0.83 V, a J_{SC} of 17.97 mA/cm^2, and a FF of 65.32%. After annealing the active layer at 150 $^{\circ}$C for 10 mins, the PCE significantly increased from 9.72% to 11.07% with a V_{OC} of 0.83 V, a remarkable J_{SC} of 20.11 mA/cm^2, and a FF of 66.16%.

The improved PCE is mainly attributed to the enhanced J_{SC} from 17.97 mA/cm^2 to 20.11 mA/cm^2. It is believed that the annealing treatment significantly improved the structural order, aggregation and morphology of the active layer, and consequently contributed to the higher J_{SC}. The J_{SC} and V_{OC} of **6TIC** system are also significantly improved compared with our recently reported **4TIC** system which has J_{SC} of 18.75 mA/cm^2 and V_{OC} of 0.78 V.[30] The higher J_{SC} and V_{OC} of **6TIC** are ascribed to its red-shifted and broadened absorption and slightly higher LUMO energy level than the **4TIC**. Considering the NIR absorption of **6TIC**, it is expected to be a promising active material for semitransparent OSCs. To demonstrate the concept, we here also fabricated a semitransparent OSC based on **PTB7-Th: 6TIC** and showed a quite high PCE of 7.62% with an average visible transmittance of 23.3% (see **Figure S1**).

From the literature, OSC devices with a high J_{SC} over 20 mA/cm^2 usually display very low V_{OC} (< 0.5V) with high V_{OC} loss (> 0.6V), resulting in modest PCE. Our result successfully demonstrates that a high PCE (> 11%), J_{SC} (> 20 mA/cm^2), V_{OC} (0.831 V), and low V_{OC} loss ($\approx$0.55 V) can be achieved simultaneously.

EQE measurements of devices without and with annealing were conducted and the corresponding curves are presented in **Figure 3b**. The two devices show the EQE responses from 350 to 900 nm, indicating **PTB7-Th** polymer donor and **6TIC** acceptor simultaneously contribute to the whole J_{SC} values. The EQE values for the annealed devices are much higher than those without annealing, reaching a maximum value around 76%, indicating efficient charge generation and collection. The higher EQE values for annealed device should mainly due to the improved structural order and aggregation of the active layer. This is proven by the significantly enhanced absorption of the active layer after being annealed at 150 $^{\circ}$C (see **Figure S2**). The J_{SC} values calculated from the EQE curves are 17.19 and 19.20 mA/cm^2 for the devices without and with annealing, respectively, which are within

reasonable mismatch to the J_{SC} values obtained from the corresponding J-V curves. The EQE measurement of semitransparent device was also conducted and the corresponding curve is presented in **Figure 3b**. As expected, the device with an average visible transmittance of 23.3%, its EQE values dropped significantly, resulting in a modest calculated J_{SC} of 14.01 mA/cm^2.

To explore the charge generation and extraction properties of the devices, the light intensity dependent J_{SC} and V_{OC} were studied. As shown in **Figure 3c**, the J_{SC} for annealed device shows an index of 0.97 with the light intensity, which is higher than 0.95 obtained for the unannealed device. The close to unity light intensity dependence (α value) in annealed device indicates insignificant charge recombination loss during charge extraction, which further supports the obtained higher J_{SC} and FF in device after annealing.[33] Further, the V_{OC} versus light intensity study revealed that there is no clear distinction between annealed and unannealed devices in the recombination process. As can be seen in **Figure 3d**, the annealed device displays a slope of 1.88 (kT/q), where the as-cast device shows a slope of 1.95 (kT/q). These data indicate that monomolecular recombination and bimolecular recombination both exit in the as-cast device and annealed device.[34]

The electron mobility of the blended films was measured using the SCLC method with the device structure ITO/ZnO/Active layer/C60-bissalt/Ag (see **Figure S3**). The as-cast device showed an electron mobility as high as 6.2×10^{-4} cm^2/V s. After annealing, the electron mobility enhanced to 7.0×10^{-4} cm^2/V s. The slightly increased electron mobility is attributed to the improved structural order of the active layer after annealing, which also account for the increased fill factor. It can also facilitate better charge extraction to result in lower recombination loss.

In order to better understand the annealing effect on the device, the morphology including the structure order, phase segregation, and surface topology of thin films was investigated by grazing incidence wide-angle x-ray scattering (GIWAXS), resonant soft x-ray scattering (RSoXS), and atomic force microscope (AFM). Shown in **Figure 4a-b** are GIWAXS pattern and line-cut profiles. **6TIC** in neat film showed a face-on orientation. An obvious π-π stacking was seen in out-of-plane direction at 1.75 Å^{-1} (3.59 Å) with a crystal coherence length of 16.2 Å.[35] An amorphous halo at ~1.3 Å^{-1} was seen, indicating a poor structure order of pure **6TIC** film. In in-plane direction, a quite weak and broad scattering peak was seen around 0.36 Å^{-1}; and a sharp peak was recorded at 0.46 Å^{-1} (13.65 Å), with a crystal coherence length of 276.1 Å. The sharp diffraction peak was ascribed to the lamellae packing of **6TIC**, forming good packing of crystallites in face-on orientation. The BHJ thin film GIWAXS results are composed of diffraction features of **PTB7-Th** and **6TIC**. In as cast thin film, quite broad polymer (100) diffraction was recorded in in-plane direction (0.28 Å^{-1}) with a crystal coherence length of 66.5 Å. The **6TIC** lamellae packing coherence length in in-plane direction was estimated to be 115.5 Å. Thus, the presence of **PTB7-Th** reduced the crystal size of **6TIC** acceptor. The π-π stacking region was composed of both **PTB7-Th** and **6TIC** diffraction features, which was hard to split and give an averaged peak position at 1.70 Å^{-1}. When thermal annealed at 150 °C for 10 min, the scattering feature remained similar with only slight change in crystal size scales. **PTB7-Th** in-plane (100) coherence length was increased to 70.6 Å, and the **6TIC** lamellae packing coherence length was increased to 128.4 Å. The improved crystal sizes helped to enhance charge transport device performance.

The length scale of phase separation was investigated by RSoXS using 285 eV photon energy that give the best contrast. The similarity in chemical structure led to a poor contrast factor when compared with that of PCBM blends, and thus a weak phase separation was seen. For as cast BHJ thin film, a quite

broad scattering with low intensities was seen from 0.003 Å^{-1} to 0.01 Å^{-1}, giving a distance of ~60-200 nm.[36-40] Thermal annealing did not help form better-defined scattering peaks. However, the scattering intensity increased significantly, and thus the extent of phase separation drastically improved. The scattering hump also shifted slightly to lower q region, giving enlarged phase separation. These results suggest that thermal annealing could induce material demixing for **PTB7-Th:6TIC** blends, and the crystallization of each component help form better transporting network to efficiently harvest solar energy.

It should be noted that thermal annealing can improve the structure order and phase separation of **PTB7-Th:6TIC** blends, which is quite different from **PTB7-Th**:PCBM systems, which when heated, would lead to worsen morphology and reduced device performance.[41] It should also be noted that the crystallites structure for **6TIC** is different from the **ITIC** analogue, which complicated crystal structure or polymorph crystallites is in the blends. The ~0.5 Å^{-1} diffraction peak in **ITIC** materials is usually appeared in the same direction to its π-π stacking peaks, made it hard to use the simple crystal unit cell to analyze the results.[42] The current **6TIC** with a well-defined lamellae diffraction orthogonal to the π-π stacking peak direction, indicating its crystal form is similar to many conjugated polymers, and thus a stabilized crystalline structure is observed in both as cast and annealed BHJ blends.

The surface morphology is also studied by AFM in tapping mode imaging, with results shown in **Figure S4**. Similar surface topology was seen for both as cast and annealed BHJ blends, and they were quite smooth in height images. The phase image showed a quite good fibril network structures regardless of the sample preparation conditions. After annealing, larger aggregation domains were observed in the phase image (see **Figure S4**), which is consistent with the RSoXS data. Such a morphology with enhanced crystalline order in annealed BHJ blends gave rise to improved device performance.

3. Conclusion

In summary, a new low bandgap fused-ring electron acceptor **6TIC** has been rationally designed and synthesized by developing a novel terthieno[3,2-*b*]thiophene (**6T**) core. The rigid and extended π-conjugation of **6T** core with electron-rich nature endows **6TIC** to have distinctive properties, such as narrowed bandgap, better molecular packing, and higher SCLC charge mobility. Consequently, the optimized device based on **PTB7-Th:6TIC** exhibits a high PCE of 11.07% with a high J_{SC} of 20.11 mA/cm^2, a high V_{OC} of 0.83 V, and a relatively low V_{OC} loss (≈0.55 V). This is a rare case to simultaneously achieve all desirable properties in the same low bandgap FREA derived devices. Moreover, for the concept demostration, a semitransparent solar cell based on **PTB7-Th:6TIC** was fabricated and exhibited a quite high PCE of 7.62%. These promising results show **6TIC** as a very

WILEY-VCH

promising low bandgap electron acceptor for applications in tandem solar cells and semitransparent solar windows.

4. Experimental Section

Chemicals and Instrumentations: All reagents were purchased from commercial sources and used without further purification. Anhydrous dichloromethane (DCM) and *N,N*-dimethylformamide (DMF) were distilled from CaH2. Anhydrous toluene and THF were distilled from sodium benzophenone immediately prior to use. The ^{1}H NMR and ^{13}C NMR spectra were recorded in solution of CDCl$_3$ on Bruker DRX 300 NMR spectrometer with tetramethylsilane (TMS) as the internal standard. High resolution (HR) MALDI-TOF mass spectra were recorded on AutoFlex II mass spectrometer. UV-vis-NIR absorption spectra were recorded on a Varian Cary 5000. The electrochemical measurements were carried out in anhydrous DCM with 0.1 M tetrabutylammonium hexafluorophosphate (Bu$_4$NPF$_6$) as the supporting electrolyte at room temperature under the protection of nitrogen. A gold disk was used as working electrode, platinum wire was used as counting electrode, and Ag/AgCl (3M KCl solution) was used as reference electrode. The potential was calibrated against the ferrocene/ferrocenium couple.

Synthesis of compound 3: Diethyl 2,5-dichlorothieno[3,2-*b*]thiophene-3,6-dicarboxylate **1** (1.41 g, 4.0 mmol), and tributyl(thieno[3,2-*b*]thiophen-2-yl)stannane **2** (3.78 g, 8.8 mmol) were dissolved in toluene (50 mL). Pd(PPh$_3$)$_4$ (140 mg) was added as a catalyst and the mixture was refluxed for 12 h under argon. After cooling down cold methanol was added and a yellow precipitate was formed. The crude product **3** was collected by filtration and used for

the next step without further purification. Both ^{1}H NMR and ^{13}C NMR data were not obtained due to its poor solubility. MALDI-TOF MS: calcd for $C_{24}H_{16}O_4S_6$ (M+), 559.9373; found, 559.9392 (error: -3.39 ppm).

Synthesis of compound 6T: A flame dried flask equipped with a stir bar was charged with Mg turnings (0.144 g, 6 mmol), anhydrous THF (20 mL) and 4-hexyl-1-bromobenzene (1.45 g, 6.0 mmmol). The above mixture was heated to reflux until the Mg turnings totally disappeared. After cooling to room temperature, compound **3** (561 mg, 1.0 mmol) was added as solid in one portion. After this addition, the mixture was slowly heated to reflux for overnight. The reaction was quenched with 10% HCl solution (10 ml) and extracted twice with ethyl acetate. The organic layer was dried (Na_2SO_4), filtered, and evaporated to dryness under vacuum. After that the crude diol was dissolved in anhydrous toluene (100 mL) and the whole system was degassed via three freeze-thaw pump cycles. To the mixture, an excess of amberlyst 14 (about 0.3 g) was added in onel portion under argon atmosphere. The mixture was heated to 80 ^{o}C for 4 hours. After that the reaction was extracted with ethyl acetate, the organic layer was dried (Na_2SO_4), filtered, and concentrated under vacuum. The residue was purified by column chromatography (silica gel, hexane: DCM 5:1 v/v). Compound **6T** was further purified by recrystallization from MeOH/CH_2Cl_2 as a yellow solid (810 mg, 75% yield for two steps). ^{1}H NMR (300 MHz, CDCl$_3$, ppm): δ = 7.25 (d, *J* = 5.2 Hz, 2H), 7.21 (d, *J* = 5.2 Hz, 2H), 7.16 (d, *J* = 8.1 Hz, 8H), 7.09 (d, *J* = 8.2 Hz, 8H), 2.54 (t, *J* = 7.8 Hz, 8H), 1.65-1.48 (m, 8H), 1.38-1.20 (m, 24H), 0.91-0.78 (m, 12H); ^{13}C NMR (75 MHz, CDCl$_3$, ppm): δ = 147.97, 146.83, 142.07, 140.27, 138.92, 138.31, 137.52, 134.84, 134.08, 128.67, 127.94, 125.51, 120.22, 62.25, 35.61, 31.67, 31.16, 29.15, 22.56, 14.05; MALDI-TOF MS: calcd for $C_{68}H_{72}S_6$ (M$^+$), 1080.3958; found, 1080.3958 (error: 0 ppm).

Synthesis of compound 6T-CHO: Compound **6T** (540 mg, 0.5 mmol) was dissolved in DMF (10 mL) and 1,2-dichloroethane (10 mL). An excess amount of phosphorus oxychloride (1 mL) was added and the mixture was stirred at 80 °C overnight. The reaction was quenched with saturated sodium acetate solution (10 ml) and stirred for 30 min at room temperature. The mixture was extracted twice with DCM, the organic layer was dried (Na_2SO_4), filtered, and concentrated under vacuum. The residue was purified by column chromatography (silica gel, hexane: DCM 1:2 v/v). Compound **6T-CHO** was further purified by recrystallization from MeOH/CH_2Cl_2 as a red solid (529 mg, 93% yield). ^{1}H NMR (300 MHz, CDCl$_3$, ppm): δ = 9.87 (s, 2H), 7.91 (s, 2H), 7.13 (s, 16H), 2.56 (t, *J* = 7.7 Hz, 8H), 1.68-1.51 (m, 8H), 1.45-1.20 (m, 24H), 0.95-0.80 (m, 12H); ^{13}C NMR (75 MHz, CDCl$_3$, ppm): δ =182.50, 150.66, 147.26, 145.45, 143.48, 142.68, 140.37, 140.29, 138.24, 137.20, 136.43, 129.67, 128.98, 127.70, 62.41, 35.59, 31.65, 31.15, 29.10, 22.54, 14.03; MALDI-TOF MS: calcd for $C_{70}H_{72}O_2S_6$ (M$^+$), 1136.3857; found, 1136.3847 (error: -0.88 ppm).

Synthesis of compound 6TIC: Compound **6T-CHO** (170 mg, 0.15 mmol) and 3-(dicyanomethylidene)indan-1-one **IC** (117 mg, 0.6 mmol) were dissolved in 1,2-dichloroethane (12 mL) and EtOH (6 mL). A catalyst amount of beta-alanine was added and the mixture was stirred at 80 °C overnight. After cooling down, the reaction mixture was concentrated under vacuum. The residue was purified by column chromatography (silica gel, hexane: DCM 1:2 v/v). Compound **6TIC** was further purified by recrystallization from EtOH/CH_2Cl_2 as a dark green solid (201 mg, 90% yield). ^{1}H NMR (300 MHz, CDCl$_3$, ppm): δ = 8.90 (s, 2H), 8.68 (d, *J* = 7.8 Hz, 2H), 8.05-7.94 (m, 4H), 7.86-7.77 (m, 4H), 7.38-7.28 (m, 16H), 2.69 (t, *J* = 7.7 Hz, 8H), 1.78-1.68 (m, 8H), 1.52-1.30 (m, 24H), 1.05-0.92 (m, 12H); ^{13}C NMR (75 MHz, CDCl$_3$, ppm): δ =188.19, 160.02, 152.53, 149.16, 148.26, 147.12, 143.00,

142.58, 139.93, 139.55, 138.97, 137.78, 136.97, 136.83, 136.73, 134.97, 134.28, 129.20, 127.79, 127.57, 125.09, 123.56, 121.92, 114.77, 114.67, 68.76, 62.51, 35.61, 31.67, 31.19, 29.15, 22.55, 14.04; MALDI-TOF MS: calcd for $C_{94}H_{80}N_4O_2S_6$ (M^+),1488.4606; found, 1488.4632 (error: 1.75 ppm).

Device Fabrication: The ITO glass substrates were cleaned via ultra-sonication in detergent solution, DI-water, acetone, and isopropanol, sequentially. After blowing dry with N_2 flow, the substrates were further cleaned by UV-Ozone machine. ZnO precursor solution (1.1 g $ZnO(Ac)_2 2H_2O$ dissloved in 10 ml mexoyethanol and 0.305 ml ethanolamine) were spin-coated on as-prepared substrate, and baked at 150 ^{o}C for 20 min in air. Active layer was deposited onto the ZnO via spin-coating in glove-box. The active layer solution is composed of 25 mg **PTB7-Th:6TIC** (1:1.5 wt%) in 1 ml chlorobenzene mixed with 0.25% DIO. The devices were completed by depositing 6 nm MoO_3 and 150 nm Ag in a vacuum chamber with a base pressure of 10^{-7} Torr. Shadow masks with an area of 0.0314 cm^2 were used to determine the device area.

Device Characterization: The I-V characteristic curves were recorded in a Keithley 2400 source unit under a simulated solar irradiance (solar simulator from Newport Inc.) A certified silicon diode, which can be traced back to NREL, is used to calibrate the illumination intensity to 1 sun (100 mW/cm^2). A neutral filter is used to study the light intensity dependent device performance. EQE spectra were measured in a assembled setup including a stable light source, light chopper, monochromator, and lock-in amplifier.

Supporting Information

Supporting Information is available from the Wiley Online Library or from the author.

Received: ((will be filled in by the editorial staff))
Revised: ((will be filled in by the editorial staff))
Published online: ((will be filled in by the editorial staff))

References

[1]   C. B. Nielsen, S. Holliday, H.-Y. Chen, S. J. Cryer, I. McCulloch, *Acc. Chem. Res.* **2015**, *48*, 2803.

[2]   Y. Lin, X. Zhan, *Adv. Energy Mater.* **2015**, *5*, 1501063.

[3]   Y. Lin, J. Wang, Z. Zhang, H. Bai, Y. Li, D. Zhu, X. Zhan, *Adv. Mater.* **2015**, *27*, 1170.

WILEY-VCH

[4]   Y. Lin, Z.-G. Zhang, H. Bai, J. Wang, Y. Yao, Y. Li, D. Zhu, X. Zhan, *Energy Environ. Sci.* **2015**, *8*, 610.

[5]   Y. Lin, X. Zhan, *Acc. Chem. Res.* **2016**, 49, 175.

[6]   Y. Xu, C. Chueh, H. Yip, F. Ding, Y. Li, C. Li, X. Li, W. Chen, A. K. Jen, *Adv. Mater.* **2012**, 24, 6356.

[7]   Y. Yang, Z. G. Zhang, H. Bin, S. Chen, L. Gao, L. Xue, C. Yang, Y. Li, *J. Am. Chem. Soc.* **2016**, *138*, 15011.

[8]   Y. Lin, Q. He, F. Zhao, L. Huo, J. Mai, X. Lu, C. J. Su, T. Li, J. Wang, J. Zhu, Y. Sun, C. Wang, X. Zhan, *J. Am. Chem. Soc.* **2016**, *138*, 2973.

[9]   Y. Lin, F. Zhao, Q. He, L. Huo, Y. Wu, T. C. Parker, W. Ma, Y. Sun, C. Wang, D. Zhu, A. J. Heeger, S. R. Marder, X. Zhan, *J. Am. Chem. Soc.* **2016**, *138*, 4955.

[10]   Y. Li, D. Qian, L. Zhong, J. D. Lin, Z. Q. Jiang, Z. G. Zhang, Z. Zhang, Y. Li, L. S. Liao, F. Zhang, *Nano Energy* **2016**, *27*, 430.

[11]   B. Kan, H. Feng, X. Wan, F. Liu, X. Ke, Y. Wang, Y. Wang, H. Zhang, C. Li, J. Hou, Y. Chen, *J. Am. Chem. Soc.* **2017**, *139*, 4929.

[12]   Y. Li, L. Zhong, B. Gautam,H. J. Bin, J. D. Lin, F. P. Wu, Z. Zhang, Z. Q. Jiang, Z. G. Zhang, K. Gundogdu, Y. Li, L. S. Liao, *Energy Environ. Sci.* **2017**, *10*, 1610.

[13]   S. Li, L. Ye, W. Zhao, S. Zhang, S. Mukherjee, H. Ade, J. Hou, *Adv. Mater.* **2016**, *28*, 9423.

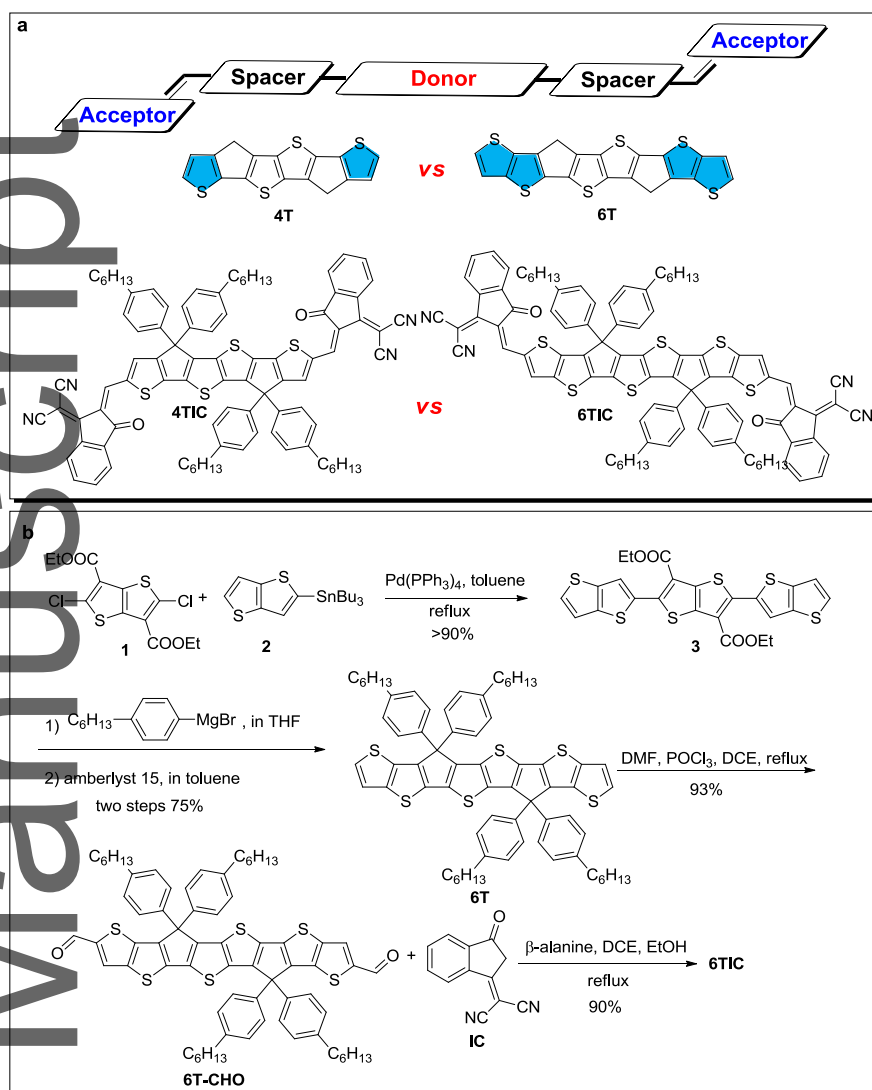[14]   Y. Wu, H. Bai, Z. Wang, P. Cheng, S. Zhu, Y. Wang, W. Ma, X. Zhan, *Energy Environ. Sci.* **2015**, *8*, 3215.
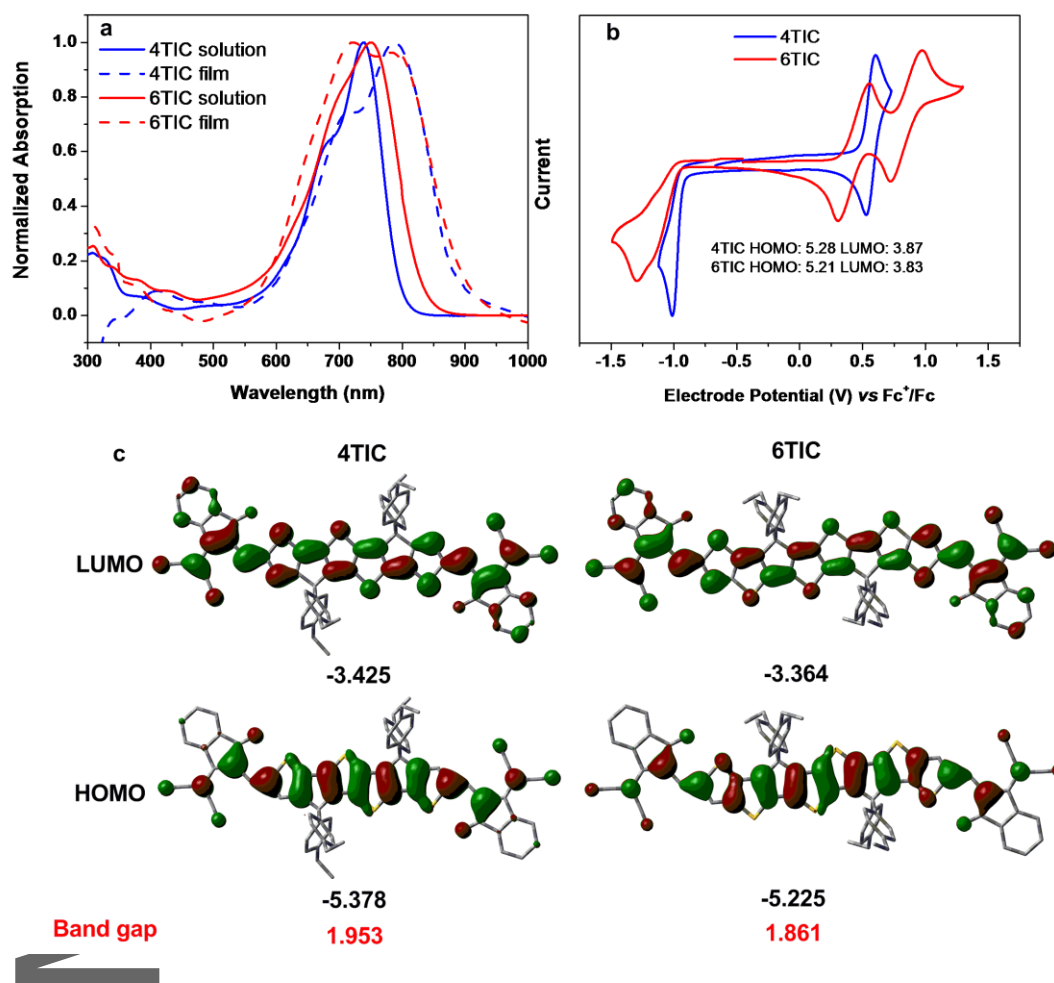
WILEY-VCH

[15]   D. Baran, T. Kirchartz, S. Wheeler, S. Dimitrov, M. Abdelsamie, J. Gorman, R. Ashraf, S.

Holliday, A. Wadsworth, N. Gasparini, P. Kaienburg, H. Yan, A. Amassian, C. J. Brabec, J.

Durrant, I. McCulloch, *Energy Environ. Sci.* **2016**, *9*, 3783.

[16]   Y. Liu, Z. Zhang, S. Feng, M. Li, L. Wu, R. Hou, X. Xu, X. Chen, Z. Bo, *J. Am. Chem. Soc.* **2017**,

139, 3356.

[17]   S. Dai, F. Zhao, Q. Zhang, T.-K. Lau, T. Li, K. Liu, Q. Ling, C. Wang, X. Lu, W. You, X. Zhan, *J. Am.

Chem. Soc.* **2017**, *139*, 1336.

[18]   F. Liu, Z. Zhou, C. Zhang, T. Vergote, H. Fan, F. Liu, X. Zhu, *J. Am. Chem. Soc.* **2016**, *138*, 15523.

[19]   H. T. Bai, Y. F. Wang, P. Cheng, J. Y. Wang, Y. Wu, J. H. Hou, X. W. Zhan, *J. Mater. Chem. A*

2015, *3*, 1910.

[20]   S. Holliday, R. S. Ashraf, A. Wadsworth, D. Baran, S. A. Yousaf, C. B. Nielsen, C.-H. Tan, S. D.

Dimitrov, Z. Shang, N. Gasparini, M. Alamoudi, F. Laquai, C. J. Brabec, A. Salleo, J. R. Durrant,

I. McCulloch, *Nat. Commun.* **2016**, *7*, 11585.

[21]   Z. Zhang, W. Liu, T. Rehman, H. X. Ju, J. Mai, X. Lu, M. Shi, J. Zhu, C.-Z. Li, H. Chen, *J. Mater.

Chem. A* **2017**, *5*, 9649.

[22]   H. Yao, L. Ye, J. Hou, B. Jang, G. Han, Y. Cui, G. M. Su, C. Wang, B. Gao, R. Yu, H. Zhang, Y. Yi, H.

Y. Woo, H. Ade, J. Hou, *Adv. Mater.* **2017**, *29*, 1700254.

[23]   Z. Xiao, X. Jia, D. Li, S. Wang, X. Geng, F. Liu, J. Chen, S. Yang, T. P. Russell, L. Ding, *Sci. Bull.*

2017, DOI: https://doi.org/10.1016/j.scib.2017.10.017.

WILEY-VCH

[24]   W. Zhao, S. Li, H. Yao, S. Zhang, Y. Zhang, B. Yang, J. Hou, *J. Am. Chem. Soc.* **2017**, *139*, 7148.

[25]   Y. Cui, H. Yao, B. Gao, Y. Qin, S. Zhang, B. Yang, C. He, B. Xu, J. Hou, *J. Am. Chem. Soc.* **2017**, *139*, 7302.

[26]   K. H. Hendriks, W. Li, M. M. Wienk, R. A. J. Janssen, *J. Am. Chem. Soc.* **2014**, *136*, 12130.

[27]   H. Yao, Y. Chen, Y. Qin, R. Yu, Y. Cui, B. Yang, S. Li, K. Zhang, J. Hou, *Adv. Mater.* **2016**, 8283.

[28]   H. Yao, Y. Cui, R. Yu, B. Gao, H. Zhang, J. Hou, *Angew. Chemie Int. Ed.* **2017**, 56, 3045.

[29]   F. Liu, Z. Zhou, C. Zhang, J. Zhang, Q. Hu, T. Vergote, F. Liu, T. P. Russell, X. Zhu, *Adv. Mater.* **2017**, *29*, 1606574.

[30]   X. Shi, L. Zuo, S. B. Jo, K. Gao, F. Lin, F. Liu, A. K-Y. Jen, *Chem. Mater.* **2017**, *29*, 8369.

[31]   T. Kunz, P. Knochel, *Chem. - A Eur. J.* **2011**, *17*, 866.

[32]   X. Shi, J. Chang, C. Chi, *Chem. Commun.* **2013**, *49*, 7135.

[33]   C. M. Proctor, M. Kuik, T.-Q. Nguyen, *Prog. Polym. Sci.* **2013**, *38*, 1941.

[34]   S. R. Cowan, A. Roy, A. J. Heeger, *Phys. Rev. B* **2010**, *82*, 241207.

[35]   K. Gao, W. Deng, L. Xiao, Q. Hu, Y. Kan, X. Chen, C. Wang, F. Huang, J. Peng, H. Wu, X. Peng, Y. Cao, T. P. Russell, F. Liu, *Nano Energy* **2016**, *30*, 639.

[36]   C. Zhou, G. Zhang, C. Zhong, X. Jia, P. Luo, R. Xu, K. Gao, X. Jiang, F. Liu, T. P. Russell, F. Huang, Y. Cao, *Adv. Energy Mater.* **2017**, 1601081.
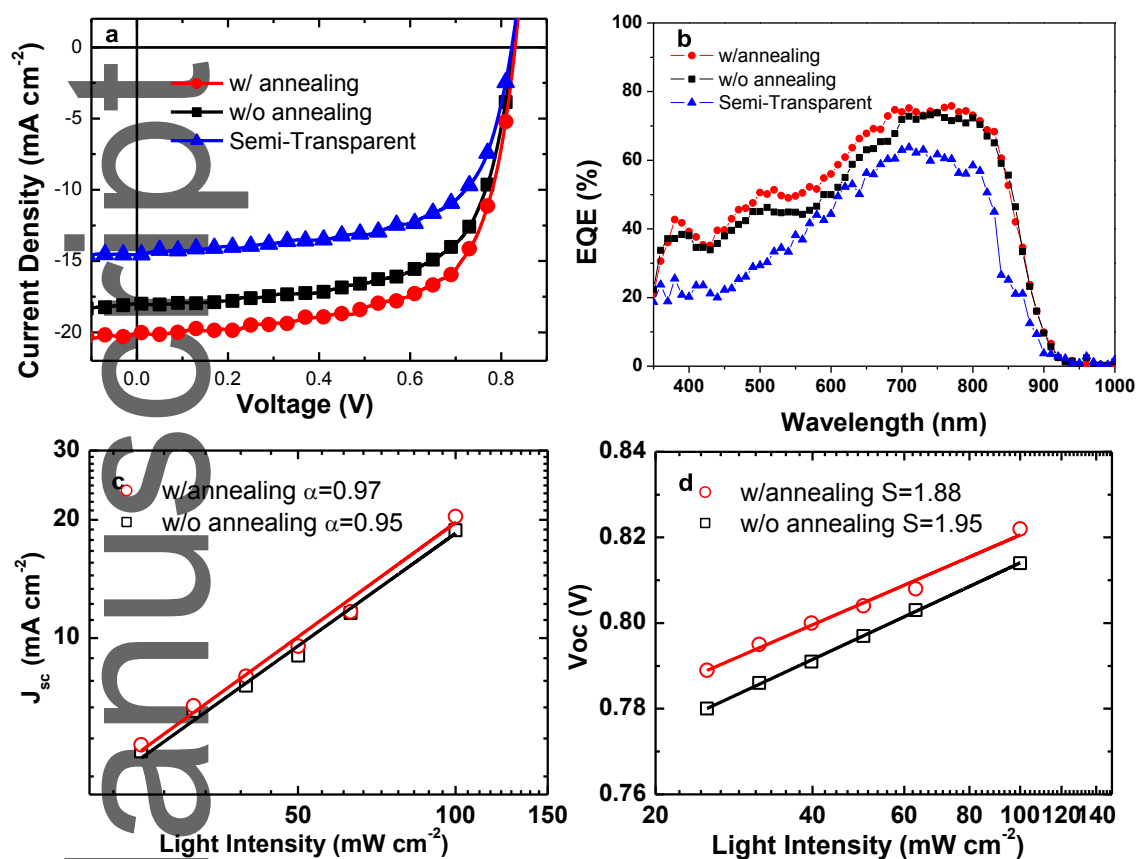
WILEY-VCH

[37]   K. Gao, J. Miao, L. Xiao, W. Deng, Y. Kan, T. Liang, C. Wang, F. Huang, J. Peng, Y. Cao, F. Liu, T.
        P. Russell, H. Wu, X. Peng, *Adv. Mater.* **2016**, *28*, 4727.

[38]   J. Wang, W. Wang, X. Wang, Y. Wu, Q. Zhang, C. Yan, W. Ma, W. You, X. Zhan, *Adv. Mater.*
        2017, *29*, 1702125.

[39]   F. Liu, M. A. Brady, C. Wang, *Eur. Polym. J.* **2016**, *81*, 555.

[40]   X. Jiao, L. Ye, A. Ade, *Adv. Energy Mater.* **2017**, 1700084.

[41]   F. Liu, W. Zhao, J. R. Tumbleston, C. Wang, Y. Gu, D. Wang, A. L Briseno. H. Ade, T. P. Russell,
        Adv. Energy Mater. **2014**, *4*, 1301377.

[42]   H. Lu, J. Zhang, J. Chen, Q. Liu, X. Gong, S. Feng, X. Xu, W. Ma, Z. Bo, *Adv. Mater.* **2016**, *28*,
        9559.

WILEY-VCH

Figure 1. (a) Molecular design and chemical structures. (b) Synthetic route to **6TIC**.
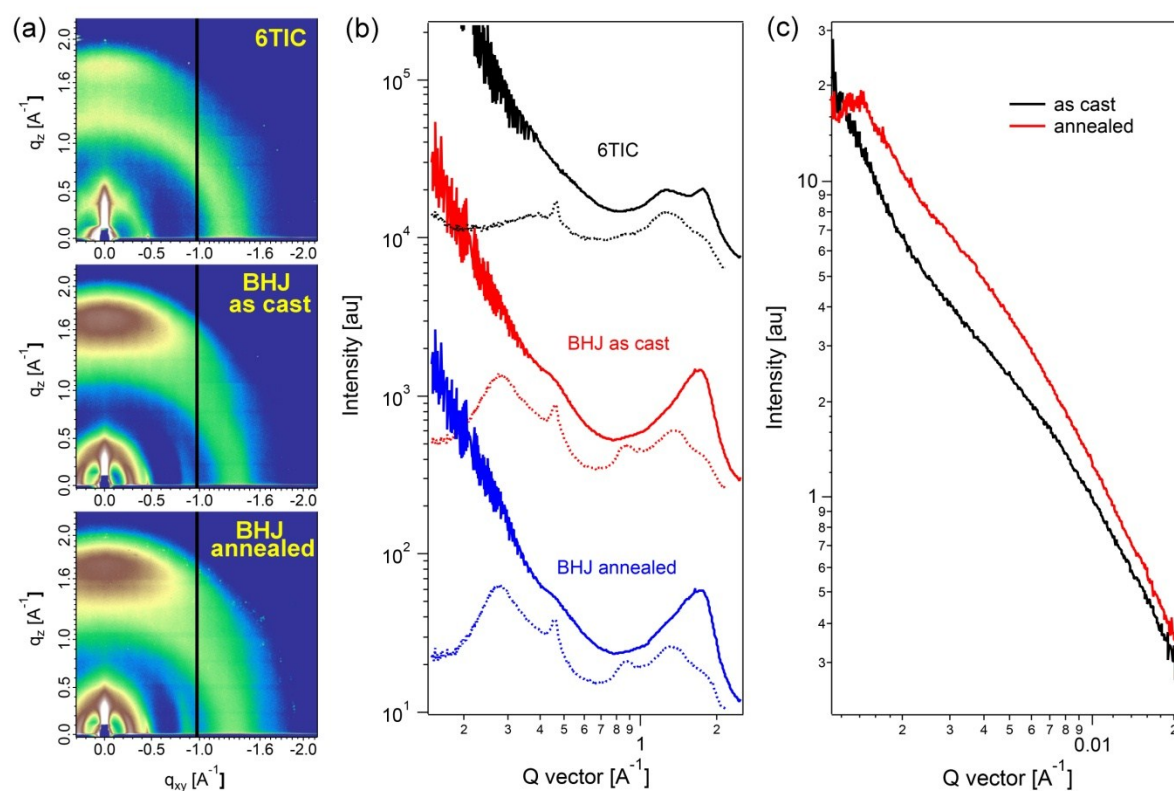
Figure 2. (a) UV-vis-NIR spectra of and **4TIC** and **6TIC** recorded in dichloromethane and in thin film. (b) Cyclic voltammograms of **4TIC** and **6TIC** in DCM with 0.1 M Bu_4NPF_6 as supporting electrolyte, Ag/AgCl as reference electrode, Pt wire as counter electrode, and scan rate at 20 mV/s. (c) simulated molecular geometries and frontier molecular orbitals obtained by DFT calculations for **4TIC** and **6TIC**.

Figure 3. (a) J-V curves of the devices based on **PTB7-Th:6TIC** without and with annealing, and semi-transparent under the best performing devices. (b) EQE curves of the devices without and with annealing, and semi-transparent under the best performing devices. (c) J_{SC} versus light intensity of the devices without and with annealing. (d) V_{OC} versus light intensity of the devices without and with annealing.

WILEY-VCH

Figure 4. Grazing incidence wide-angle x-ray scattering (a) scattering pattern, (b) line-cut profiles (solid-line: out-of-plane profile; dotted-line: in-plane profile.), (c) resonant soft x-ray scattering of BHJ blends with and without thermal annealing.

Table 1. Summary of the photophysical and electrochemical data.[a]

Compound	HOMO (eV)	LUMO (eV)	E_g^{EC} (eV)	E_g^{OPT} (eV)
4TIC	-5.28	-3.87	1.41	1.40
6TIC	-5.21	-3.83	1.38	1.37

[a]HOMO= - (4.8 + E_{ox}^{onset}) and LUMO= - (4.8 + E_{red}^{onset}), where E_{ox}^{onset} and E_{red}^{onset} are the onset potentials of the first oxidative and reductive waves, respectively. E_g^{EC}: electrochemical band gap. E_g^{OPT}: optical band gap estimated from the absorption onset.

Table 2. Photovoltaic parameter of OSCs based on **PTB7-Th:6TIC**.

Device	V_{OC} (V)	J_{SC} (mA/cm^2)	FF (%)	PCE (%)[a]	Calc. J_{SC}[b] (mA/cm^2)
w/ annealing	0.831 (0.826)	20.11 (19.63)	66.16 (65.71)	11.07 (10.65)	19.20
w/o annealing	0.828 (0.826)	17.97 (17.55)	65.32 (64.89)	9.72 (9.51)	17.19
Semi-T	0.823 (0.821)	14.58 (14.03)	63.50 (61.12)	7.62 (7.17)	13.92

[a]Average values obtained from ten devices are shown in parentheses; [b]Obtained by integration of the EQE curves.
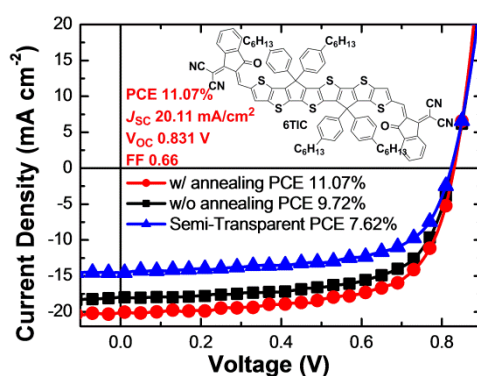
WILEY-VCH

Terthieno[3,2-*b*]thiophene (6T) based low band-gap fused-ring electron acceptor 6TIC is developed for high efficiency solar cells. The device based on PTB7-Th:6TIC blend exhibits a high PCE of 11.07% with a high J_{SC} over 20 mA/cm^2 and a high V_{OC} of 0.83 V with a relatively low V_{OC} loss (≈0.55 V). Moreover, the semitransparent solar cell based on PTB7-Th:6TIC exhibits a very promising PCE of 7.62%.

Keyword organic solar cell, non-fullerene acceptors, low band-gap semiconductor

Xueliang Shi[a,†], Jingde Chen[a,e†], Ke Gao[a,†], Lijian Zuo[a], Zhaoyang Yao[a], Feng Liu*[d], Jianxin Tang*[e], Alex K-Y. Jen*[a,b,c]

Terthieno[3,2-*b*]thiophene (6T) based low band-gap fused-ring electron acceptor for high efficiency solar cell with a high short-circuit current density and low open-circuit voltage loss

ToC figure